Supporting information

Eco-friendly plasmonic sensors: Using the photothermal effect to prepare metal nanoparticle–containing test papers for highly sensitive colorimetric detection

Shao-Chin Tseng,[a] Chen-Chieh Yu,[a] Dehui Wan,[a] Hsuen-Li Chen,[a] Lon Alex Wang,[b]*

Ming-Chung Wu,[a] Wei-Fang Su,[a] Hsieh-Cheng Han[c] , and Li-Chyong Chen[c]

[a] Department of Materials Science and Engineering, National Taiwan University,

Taipei, Taiwan

[b] Graduate Institute of Photonics and Optoelectronics, National Taiwan University,

Taipei, Taiwan

[c] Center for Condensed Matter Science, National Taiwan University, Taipei, Taiwan

No. 1, Sec. 4, Roosevelt Road, Taipei, 10617 Taiwan (R.O.C)

E-mail: hsuenlichen@ntu.edu.tw

Nanaoparticles distribution

The density and diameters of the nanoparticle distribution on paper substrates after laser annealing could be measured from the SEM images in the manuscript (Figure 2). Moreover, the images could be used to quantify the density of the nanoparticles which were formed as a function of the number of laser shots. The density of the nanoparticles as a function of the number of laser shots was summarized in Table S1. The data in Table S1 was obtained by using the software Image J, which has a built-in tool for measuring the size and number density of particles in an image. Besides, the size and number density are double-checked by measuring manually from a 2*2 μ m area. The measurements are repeated for 4 times (2 times in the center area and another 2 times in the edge area of the sample) to obtain the standard deviation. The density was 48/μm^2 at 1 shot, 227 /μm^2 at 5 shots, 318 /μm^2 at 10 shots, and 322 /μm^2 at 15 shots. When number of shots increased, the density of nanoparticles increased, and therefore we could control the density of nanoparticles by the number of laser shots. Besides, we found that the density of nanoparticles nearly became saturated when the number of laser shots exceeded 10 shots, thus we concluded that 10 shots of laser illumination was enough to obtain the maximum density of nanoparticles.

Table S1. Average size, standard deviation, and density of Au nanoparticles as a function of the number of laser irradiation shots.

Number of laser shots	Average size (nm)	Standard deviation (nm)	Density (μm^{-2})
1	108.3 (island film)	49.01	48
5	59.25	19.32	227
10	46.31	12.78	318
15	43.12	11.67	322

To prepare the test papers, we first examined the optical characteristics of various paper substrates. We compared four kinds of paper substrates: photographic paper, ink-jet printing paper, waxed paper, and nonwoven fiber sheets. The photographic paper was that typically used for printing photographs. The surface of this photographic paper was coated with a layer of polymer to make it waterproof; it was also rather smooth, leading to a highly reflective surface. Ink-jet printing paper is commonly most for documental processing; it is cheap and readily obtained. Because ink-jet printing paper is not waterproof, it readily shrinks in aqueous solutions. The waxed paper had a smooth surface in dry state and was rather transparent to light. In water, however, it became wrinkled after it had soaked. The nonwoven fiber sheets had a relatively rough surface because there were many fibers of micron to millimeter scale in the paper. Although nonwoven fiber sheets have outstanding water-proof properties, their roughness might lead to a large degree of scattering of incoming light. From measurements made using a spectrometer with an integrated sphere, we found that the photographic paper and ink-jet printing paper were highly reflective (ca. 85%, Figure S1a). Therefore, we would more likely observe the reflection signal during sensing if we were to use the ink-jet printing and photographic papers as the paper substrates. We name these kinds of substrates "reflection–type" test papers. In contrast, the waxed paper and the nonwoven fiber sheet had an obvious transmission

ca. 50% in the visible regime. Thus, we could monitor the transmittance signal when the test papers were based on waxed paper and nonwoven fiber sheets. We called these kinds substrates "transmission-type" test papers. Figures S1b-e display optical microscopy (OM) images of the four kinds of papers. The surface of the photographic paper was rather smooth (Figure S1b), leading to high reflection of light at its surface. The root-mean-square (RMS) roughness of the photographic paper substrate surface, analyzed using atomic force microscopy (AFM), was approximately 13 nm. The ink-jet printing paper had a much rougher surface than that of the photographic paper, arising from its micro-scale fibers (Figure S1c); the RMS roughness of the ink-jet printing paper's surface was approximately 4.2 μm. The waxed paper had a smooth surface in the dry state (Figure S1d), with an RMS roughness of approximately 1 μm. Generally, waxed paper is very thin (ca. 30 μm), allowing the transmission of light. The nonwoven fiber sheet had relatively rough surface (Figure S1e), with an RMS roughness greater than 9.3 μm; we expected this roughness to lead to immobilization of NPs with serious uniformity and aggregation issues.
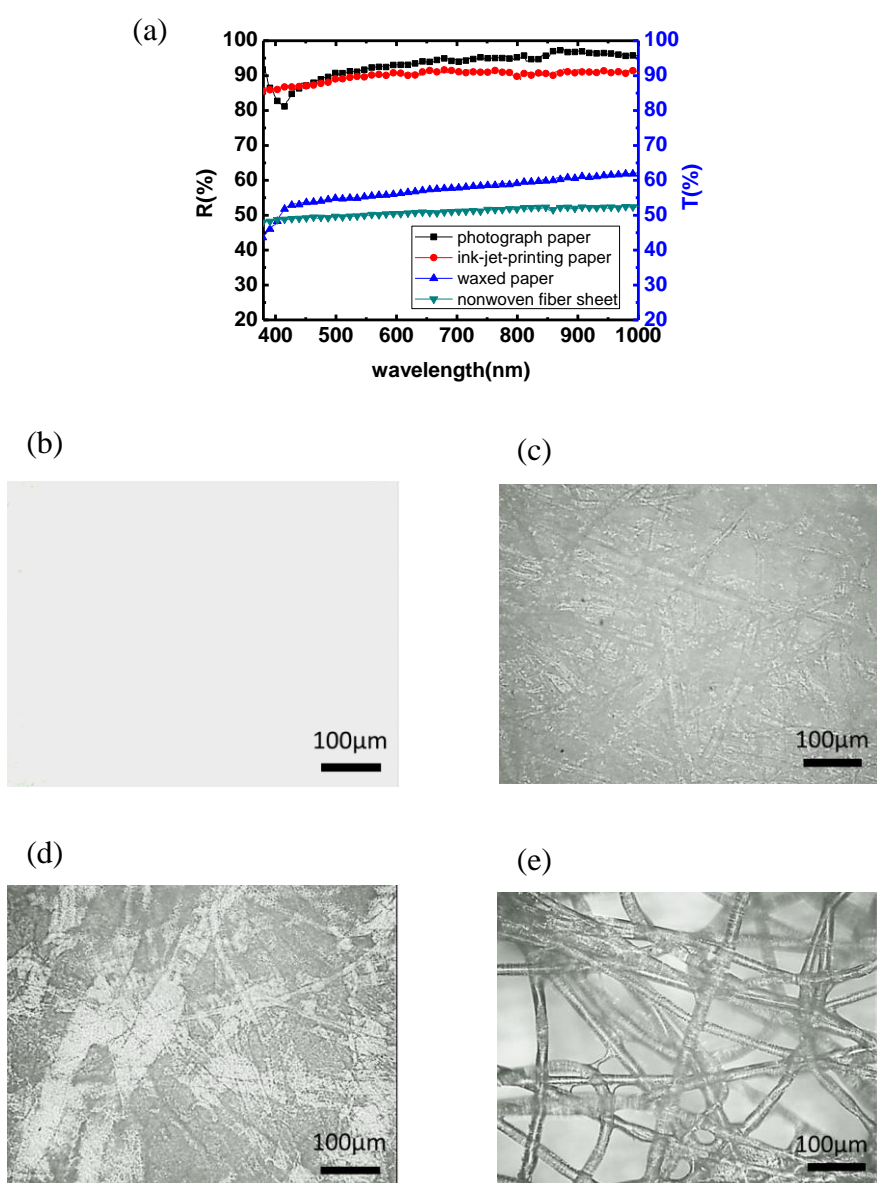
Figure S1. (a) Reflectance and transmittance spectra of various paper substrates. (b–e) Optical microscopy images of (b) photographic paper, (c) ink-jet printing paper, (d) waxed paper, and (e) nonwoven fibered sheets.

Figures S2a–h display photographic images of Au and Ag NP–containing test papers prepared using different numbers of shots of KrF excimer laser irradiation. When a thin Au film was deposited on a paper substrate, the paper featured a dark golden color—the intrinsic color of a thin Au film. After one shot of laser illumination, however, the Au film became partially transformed into an island film. The color of the Au film changed from dark golden to dark purple. The photographic images in Figures S2a–d display the Au NPs prepared on the photographic paper, ink-jet printing paper, waxed paper, and nonwoven fiber sheet, respectively. After increasing the number of shots of the laser pulse, the color of the Au film gradually changed to pink color, indicating that the Au film had transformed into Au NPs, with the pink or red color resulting from the LSPR characteristics of the Au NPs.

On the other hand, the test paper featured a dark silver color when a 15-nm-thick Ag film was deposited on it. The Ag NP-containing test paper gradually changed a dark yellow color upon increasing the number of irradiation shots (Figures S2e–h), consistent with the Ag film transforming into the particle morphology. After 10 or 15 shots, the island film transformed completely into the NP morphology. Therefore, the change in the color of the Ag film from dark silver to bright yellow revealed the transformation of the Ag film into NPs.

Next we compared the performances of the reflection-type test papers. As indicated in Figure S2, the Au and Ag NP–containing photographic papers provided a brighter and more-uniform reflected color than did the ink-jet printing paper. The photographic images revealed that this phenomenon was quite general, regardless of the number of laser shots. The ink-jet printing paper had a much rougher surface than that of the photographic paper; therefore, it featured a darker reflected color due to the scattering loss. For the transmission-type test papers, the Au (Figure S2c) and Ag (Figure S2g) NP–containing waxed papers displayed much more uniform colors than did the Au (Figure S2d) and Ag (Figure S2h) NPs on the nonwoven fiber sheets. The Au and Ag NPs provided clear pink and yellow colors, respectively, on the waxed paper; they became brighter upon increasing the number of laser shots. In contrast, the NPs on the nonwoven sheet displayed a rather dark color, with no obvious change in color observed upon increasing the number of laser shots. Because the nonwoven fiber sheet had a relatively rough surface and high porosity, it was difficult to form uniform NPs on this substrate. Thus, we concluded that the paper substrates had a relatively smooth surface would be better for fabricating test paper, either in reflection-type or transmission-type.
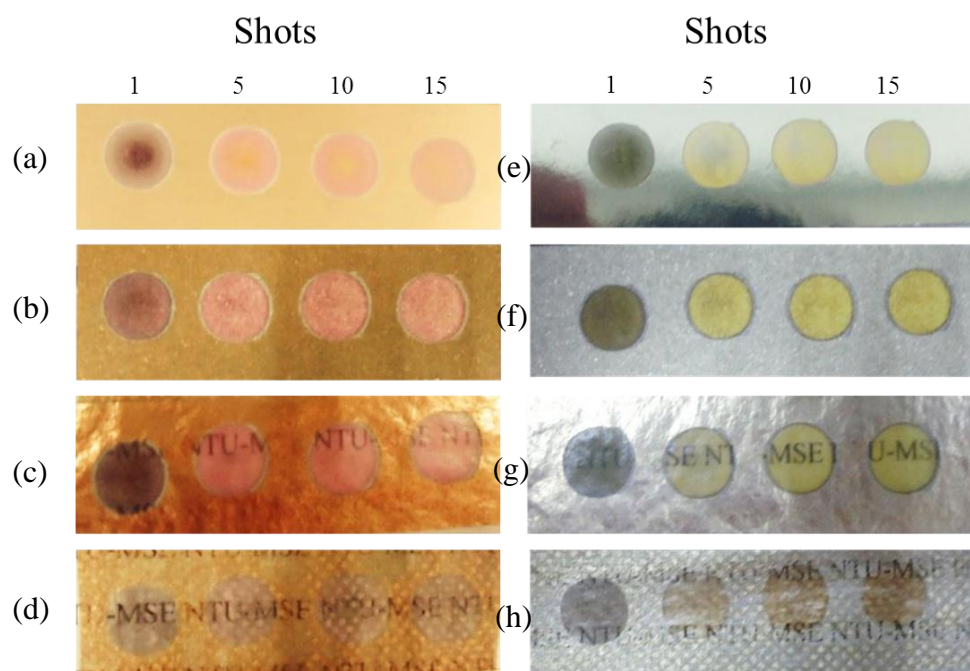
Figure S2. Photographic images of (a–d) Au NP– and (e–h) Ag NP–containing test papers prepared from (a, e) photographic paper, (b, f) ink-jet printing paper, (c, g) waxed paper, and (d, h) nonwoven fiber sheets, with different numbers of pulses of KrF laser irradiation.

Next, we investigated the biosensing ability of a reflection-type NP-containing test paper employing photographic paper as the substrate. Much biomedical research[32, 33] is focused on the detection of thiol-containing amino acids, particularly cysteine (Cys) and homocysteine, because they play various roles in, for example, acquired immune deficiency syndrome (AIDS) and cardiovascular diseases. Detection of these thiol-containing amino acids is an important aspect of both medical and pharmaceutical science.[32, 33] Previously, we have fabricated a flexible biosensor by imprinting metal NPs into a polymer substrate and developed a sensing system to detect Cys molecules.[34] Herein, we slightly modified the sensing method to fit the paper substrates. The as-fabricated NP-containing test papers were sequentially immersed in aqueous solutions of Cys (1 mM), Cu^{2+} (1 mM), and Cys-coated Au NPs (target) for 10, 10, and 30 min, respectively. All solutions were made by deionized water (DI water) except for that the target solutions were made by buffer solution. Before each immersion, the test paper was rinsed by DI water and dried by a flow of nitrogen. The Cys-coated Au NP target solution was prepared afresh prior to the immersion by mixing Cys (from 10 nM to 1 mM) and Au NPs (13.4 nM, 1:7, v/v) for 3 min. After performing a final rinse with ultrapure water, the paper sample was dried under a flow of nitrogen. All solutions and modification of NP-containing test papers were made in a glove box (fixed temperature at $25^{o}C$, nitrogen ambient). The

aggregation of the Cys-coated NPs from the target solution and onto the paper substrate induced new LSPR signals at longer wavelengths. Changing the concentration of the target solution affected the extent of aggregation and, therefore, the intensity of the LSPR peak. Figure S3a and S3b display the absorbance spectra of the Au and Ag NP–containing test papers after binding to the Cys targets. The as-prepared Au and Ag NP–containing test papers featured their LSPR peaks at 530 and 400 nm, respectively; aggregation of the Cys-coated NPs led to new LSPR peaks at 633 and 726 nm, respectively. We suspected that the Cys molecules appeared to have stronger affinity for the Ag NPs than for the Au NPs; that is, Cys molecules—and, therefore, Cu^{2+} ions also—adsorbed onto the Ag NPs strongly during the first step of the surface modification process. We infer that the Cys-modified NPs subsequently bound strongly to the Ag NPs on the paper surface, contributing to the greater degree of aggregation of the Cys-coated NPs. Therefore, the aggregation-induced absorbance signal of the Ag NP–containing test paper appeared at a longer wavelength than that of the Au NP–containing test paper. To quantitatively detect Cys molecules, we monitored the ratios of the absorption peak wavelengths A_{633}/A_{530} and A_{726}/A_{400} in the spectra of the Au and Ag NP–containing test papers, respectively, in the presence of the targets. Figure S3c and S3d indicate that the values of A_{633}/A_{530} and A_{726}/A_{400} both increased upon increasing the Cys

concentration from $1*10^{-7}$ to $1*10^{-3}$ M (Figure S3c) and from 10^{-8}M to 10^{-3}M (Figure

S3d). Moreover, we calculated the limits of detection (LOD) of our plasmonic test

papers.[35] The LOD of Ag nanoparticle-containing test papers is $2.4*10^{-9}$ M whereas

the LOD of Au nanoparticle-containing test papers is $2.1*10^{-8}$M. The detailed

calculations of LOD are provided in the last section of supporting information.

Therefore, our plasmonic papers demonstrated a low LOD down to nanomolar

conentrations. Thus, the NP-containing test paper assays exhibited sensitivity

comparable to those of previously reported colorimetric biosensors.[36-38] In addition,

we could also use these biosensors to detect Cys targets at low cost with the aid of a

scanner. We scanned the NP-containing test papers after they had bound to the Cys

targets and analyzed them using image analysis software to provide corresponding

values of their gray levels, defined herein as ranging from 255 for pure white to 0 for

pure black. Figure S3e and S3f display the gray levels of the Au and Ag

NP–containing test papers, respectively, after binding to their targets at various

concentrations. Prior to binding to the Cys targets, the Au NP–containing test paper

had an initial gray level of 171. After binding to the Cys targets at a concentration of

10^{-3} M, the gray level was 67; it gradually increased upon decreasing the

concentration of the target solution, reaching 166—a value distinct from the initial

value of 171—at a concentration to 10^{-7} M. Therefore, the detection limit for this test paper ($<10^{-7}$ M) was comparable to those of other kinds of reported biosensors.[36-38]

Similarly, in the absence of the binding targets, the Ag NP–containing test paper provided an initial gray level of 195. After binding to the Cys targets at a concentration of 10^{-3} M, the gray level decreased to 28; it gradually increased upon decreasing the concentration of the target solution. At 10^{-7} M, the gray level was 184; therefore, the variation in gray level of this test paper was still recognizable at such a low concentration. Notably, the underlying paper substrates would not contribute background signal to our colorimetric and gray level detection (Figure S4). Photographic images of the test papers after binding to different concentrations of the Cys targets (Figure S3e and S3f) reveal that distinct changes are evident to the naked eye, even at low concentration. Notably, unlike the expensive optical spectrum analysis instruments used in other assays, the equipment used with this method was merely an inexpensive home-use scanner.
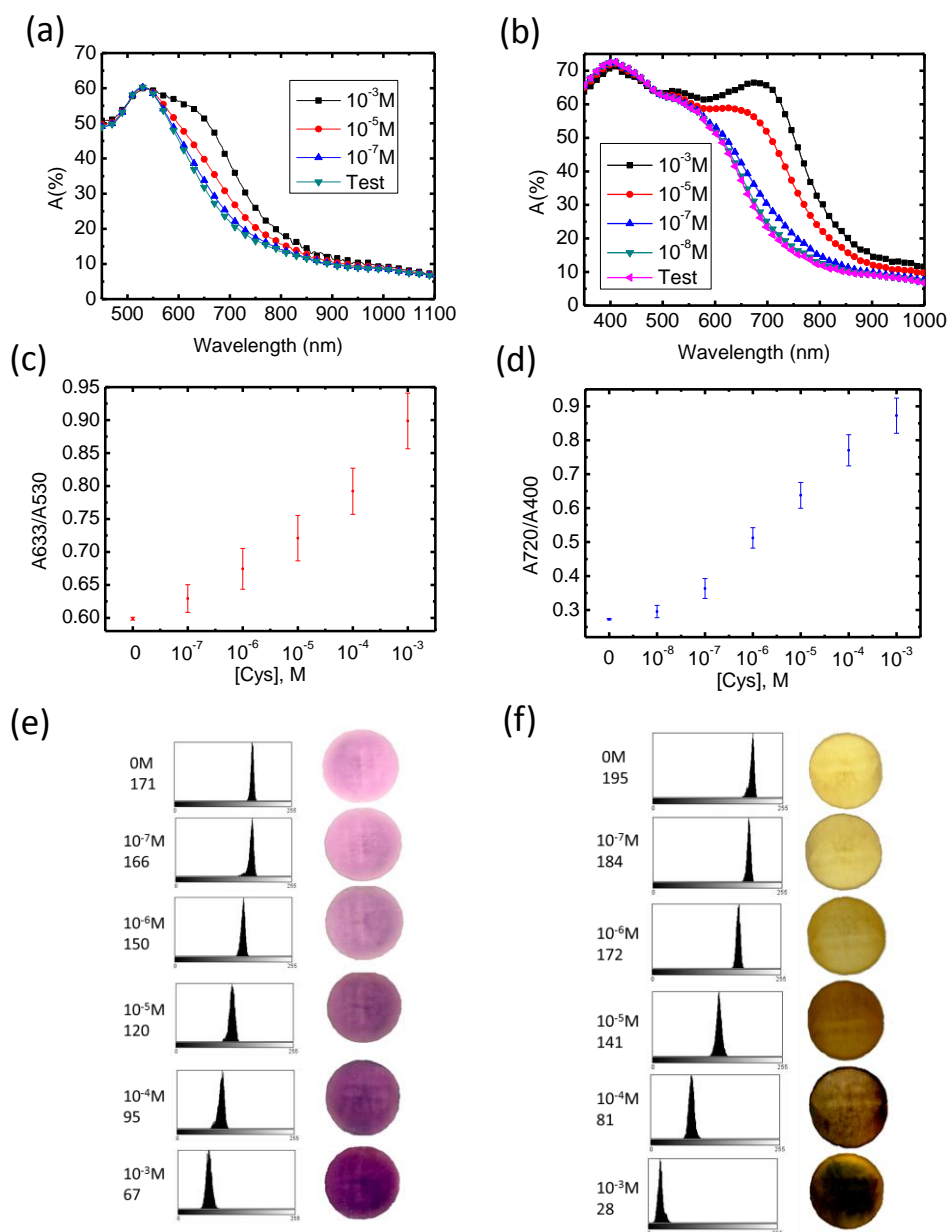
Figure S3. (a, b) Absorbance spectra of (a) Au NP– and (b) Ag NP–containing test papers at different concentrations of Cys. (c, d) Absorbance ratios of the test papers based on (c) Au NPs (A_{633}/A_{530}) and (d) Ag NPs (A_{726}/A_{400}) at different concentrations of Cys. (e, f) Gray levels and displayed colors of (e) Au NP– and (f) Ag NP–containing test papers at different concentrations of Cys.

Figure S4. provided the photograph images, absorbance spectra, and gray level value of blank photographic paper before and after binding of Cys-caoted Au NPs (10^{-3}M). There was no difference between the photographic papers before and after binding target, neither in colorimetric detection nor gray level value. Therefore, we could conclude that the underlying paper substrates would not contribute background signal to the performance of plasmonic test papers.
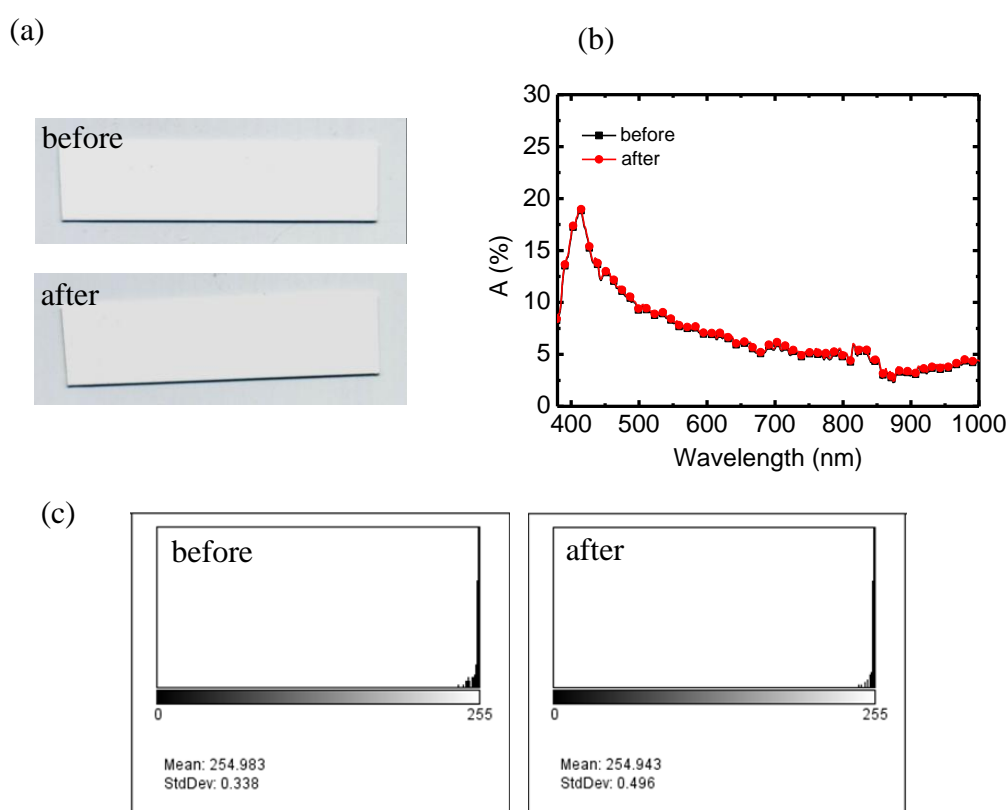

Figure S4. (a) Photograph images, (b) Absorbance spectra, and (c) gray level value of blank photographic paper before and after binding of Cys-coated Au NPs (10^{-3}M).

Calculation of limits of detection (LOD):

The limits of detection (LOD) are calculated according the following equation:

$$C_L = kS_{bi}S \tag{1}$$

where the C_L is the LOD expressed as the concentration, k is a numerical factor, S_{bi} is the standard deviation of blank measuremens, and S is the sensitivity (as defined below).

The sensitivity (S) is defined as:

$$\frac{\Delta Concentraton}{\Delta Intensity} \tag{2}$$

Therefore, the sensitivity (S) of Ag and Au nanoparticle-containing test papers are calculated using the change in A_{726}/A_{400} and A_{633}/A_{530} before and after binding of 10^{-8}M and 10^{-7}M Cys targets (Figure 3a-d), respectively. And the sensitivity of Ag and Au nanoparticle-containing test papers are $4.4*10^{-7}$M/a.u and $3.3* 10^{-6}$M/a.u.

The S_{bi} of Ag and Au nanoparticle-containing test papers are 0.0018(a.u) and 0.0021(a.u), respectively. We take the factor k =3 as the IUPAC recommended.[35] Thus, the LOD of Ag and Au nanoparticle-containing test papers are $2.4*10^{-9}$M and $2.1*10^{-8}$M, respectively.

References

(32) Jacobsen, D. W. *Clin. Chem.* **1998**, *44*, 1833-1843.

(33) Lawrence, N. S.; Davis, J.; Jiang, L.; Jones, T. G. J.; Davis, S. N.; Compton, R. G. *Analyst* **2000**, *125*, 661-663.

(34) Wan, D. H.; Chen, H. L.; Lai, Y. T.; Yu, C. C.; Lin, K. F. *Adv Funct Mater* **2010**, *20 (11)*, 1742-1749.

(35) Thomsen, V.; Schatzlein, D.; Mercuro, D. *Spectroscopy* **2003**, 18, 12, 112-114

(36) Li, B. X.; Li, L. *Analyst* **2009**, *134*, 1361-1365.

(37) Zhang, F. X.; Han, L.; Israel, L. B.; Daras, J. G.; Maye, M. M.; Ly, N. K.; Zhong, C. J. *Analyst* **2002**, *127 (4)*, 462-465.

(38) Uehara, N.; Okubo, K.; Shimada, T.; Shimizu, T. *Anal. Sci.* **2007**, *23 (1)*, 85-90.